Title
Structural Rearrangements of Subnanometer Cu Oxide Clusters Govern Catalytic Oxidation

Journal
ACS Catalysis, 10(9)

ISSN
2155-5435

Authors
Sun, Geng
Alexandrova, Anastassia N
Sautet, Philippe

Publication Date
2020-05-01

DOI
10.1021/acscatal.0c00824

Peer reviewed

Structural Rearrangements of Subnanometer Cu Oxide Clusters Govern Catalytic Oxidation

Geng Sun[1], Anastassia N. Alexandrova[2,3]*, Philippe Sautet[1, 3]*

1. Department of Chemical and Biomolecular Engineering, University of California, Los Angeles, Los Angeles, California 90095, United States

2. Department of Chemistry & Biochemistry, University of California, Los Angeles, Los Angeles, California 90095, United States

3. California Nano Systems Institute, Los Angeles, California 90095, United States

* Corresponding authors:

Anastassia N. Alexandrova: ana@chem.ucla.edu

Philippe Sautet: sautet@ucla.edu

Abstract

Sub-nanometer metal oxide clusters are very important materials, widely used for example in catalysis or electronic devices such as sensors. Hence, it is critical to understand the atomic structures and properties of sub-nanometer metal oxide clusters under a reactive gas environment, such as O_2. We consider here experimentally-accessible precise-size Cu clusters (Cu_4) supported on partial hydroxylated amorphous alumina and show that such clusters can access, in catalytic conditions at high temperature under a pressure of O_2, a large ensemble of oxidized structures, representing a large variety of oxygen content, of geometries in link with the support, and of catalytic activities for oxidation reactions, as seen from their reducibilities. A

grand canonical basin hopping method based on first-principles energy, reveals an ensemble of 24 configurations for the Cu_4O_x cluster of low free energy, less than 0.8 eV above the global minimum. The low free energy ensemble consists of clusters of different stoichiometries, which are mainly Cu_4O_3 and Cu_4O_4 in the temperature range of $200-400℃$ and under a pressure of 0.5 bar of O_2. The presence of several competitive isomers at each composition implies that cluster fluxionality impacts the phase diagram, which should be ensemble-averaged. In terms of catalytic oxidation activity, Cu_4O_3 isomers present highly variable O abstraction energy: the most stable isomers are inactive for alkane oxidative dehydrogenation, but isomerization to metastable isomers, that proceed with low barrier, enable to create active configurations with low O abstraction energy. O atoms with lowest anionic character, and thus of more electrophilic nature, present the best oxidation capability. In contrast, all Cu_4O_4 isomers show a low O abstraction energy and a high potential catalytic activity. This manuscript demonstrates the unique structural and electronic properties of sub-nano Cu oxides clusters and illustrates the critical roles of configuration ensembles and rearrangement to highly reactive metastable cluster isomers in nanocatalysis.

Keywords: grand canonical Basin Hopping, copper oxide, reconstruction, oxidative dehydrogenation, fluxionality

1 Introduction

Sub-nanometer (or sub-nano) clusters recently became very popular in heterogeneous catalysis studies because of their novel catalytic properties in many important reactions.[1-5] Similar to single atom catalysts (SACs), sub-nano clusters provide an alternative way to efficiently utilize the catalytic atoms to reduce the high cost of precious metals. In addition, in some reactions such as alkane isomerization[6], formaldehyde oxidation[7], sub-nano clusters, which consist of several active atoms, are found to be more reactive

than single-atom catalysts.[6, 8-9] Small nanoclusters are very attractive because of their specific structural and electronic properties,[10-11] which are important factors to understand their catalytic properties. However, an additional key characteristics of nanoclusters is the fluxionality, implying their ability to restructure in reaction conditions, and to access not one but an ensemble of low free energy structures. Under reaction conditions, especially at high reaction temperatures, nanoclusters are able to populate less stable configurations. Hence, nanocluster catalysts are better described as an ensemble of dynamically connected isomers rather than a single static global minimum (GM),[12-15] as seen in previous theoretical and experimental studies.[13-14, 16-19] In some cases, a metastable isomer can completely dominate the catalytic reaction rate, even though it shows a much smaller population than the GM structure.[15]

Nano copper oxide clusters are particularly interesting because of their catalytic activities in a wide range of applications, such as NO reduction,[20] CO_2 reduction[21] and especially the selective oxidation of small alkanes. One example is the selective methane oxidation to methanol [22-24] by Sebastian et al., who found that a tri-nuclear $Cu_3O_3^{2+}$ species can uniformly disperse on the side-pocket positions of a mordenite zeolite and efficiently catalyze the reaction with one order of magnitude higher activity than that of previously reported catalysts.[22] Similar catalysts can be also prepared as Cu in ZSM-5.[23-24] Besides zeolites,[25] CeO_2 has also been reported to be an efficient support. Another example of selective oxidation is alkene epoxidation.[26-28] Compared with commercialized Ag-based catalyst, Cu-based catalysts are both efficient and cheap.[29] The active sites of epoxidation reaction are still in debate[30], and in some experiments, the Cu(I) phase is proposed to be responsible for the activity of selective oxidation.[28, 31] A third example is oxidative dehydrogenation (ODH) of alkane. For example, Cu clusters are much more selective for dehydrogenation of cyclohexane to cyclohexene or benzene versus CoO_x, PdO_x, as well as bulk Cu oxide catalysts[17, 32-33]. Partial reduction

and structural changes when bound to reaction intermediate were recently underlined as important to differentiate Cu and Pd cluster selectivity.[31]

The soft-landing of size-selected clusters has been successfully used for synthesizing single-size Cu_4 clusters on various model supports, such as planar amorphous alumina and ultrananocrystalline diamond.[1, 34-35] Considering the small size of the Cu_4 oxide clusters and the low surface area of the support, characterization is very challenging. Although it is known that the oxygen contents of oxide clusters are variable under reaction conditions,[17, 36] the roles of those changes in the mechanism are unclear. In addition, if minority cluster states with highly-specific oxygen content are mechanistically-relevant, they might remain undetected in the experiment (e.g. X-ray absorption near edge structure), which measured an ensemble-average signal. Therefore, first-principles simulations provide a powerful access to investigate the properties of these Cu_4 subnano clusters and to generate insights for understanding their catalytic properties.

In this study, we exploited density functional theory (DFT) and the grand canonical basin hopping method (GCBH)[37-38] to explore the structures and reducibility of Cu_4 oxide clusters deposited on amorphous alumina (a-Al_2O_3). Structure explorations with GCBH were performed with an oxygen chemical potential corresponding to an oxygen reservoir at 0.5 bar and 200 °C, a temperature at which oxidized Cu clusters are active for selective oxidation reactions.[17] The GCBH method generates a large number of Cu_4O_x configurations and their free energies was compared on a larger range of temperature (150-500 °C was used here). Grand canonical methods[39-40] have been used in catalysis modelling, mainly using force fields for diffusion in porous materials[41-42] or for the oxidation of Pt or Pd nanoparticles[43-44]. More computational intensive simulations using first principles grand canonical approaches have recently appeared to model supported clusters in catalytic conditions[45-46]. We show that the clusters can access an ensemble of low free energy configurations, corresponding to various O content (from 2 to 5),

different structures and interaction modes with the support. These low energy configurations present markedly variable reducibilities, and thus activities for catalytic oxidation reactions. The most stable Cu_4O_3 isomer is difficult to reduce, representing a difficult step in the catalytic loop. However, metastable isomers of Cu_4O_3 are much more reducible than the most stable structure, and can be kinetically accessed at reaction temperatures, thus providing facile pathways for high catalytic activity. To calculate the electronic energy of each configuration of Cu_4O_x on the support, we rely on DFT. However, the widely used GGA functionals, such as PBE, suffer from the so-called self-interaction error in predicting semi-localized *d* orbital of Cu atoms, causing inaccuracy in the Cu oxide formation energy, and they also fail to predict the bond energy of O_2. The range separated hybrid functional HSE06 (Heyd–Scuseria–Ernzerhof),[47-48] though still failing to capture a possible multi-reference character in Cu systems, has been demonstrated to be more accurate in the prediction of thermodynamics properties such as the Cu oxide phase diagram[49] and O_2 bond energy (Supporting Information Table S1). Considering that the huge computational cost hampers exploiting multi-references method for such a large system, and that there exist good agreement between experiments and simulations using hybrid functionals for similar system[50-51], we resort to the HSE06 functional as a baseline method in the present paper. In addition, to carry out structure sampling more efficiently, we optimize the Hubbard U and chemical potential of oxygen according to the HSE06 results of the current system, to avoid the intensive HSE06 calculations in the sampling. The details are described in the Supporting Information. In the following, we first discuss the diverse structures and compositions of the low free energy Cu_4O_x clusters. Then the impact of cluster fluxionality on the oxidation reaction activities is presented and analyzed in terms of the local coordination and electronic structure of the Cu atoms.

2 Structural and stoichiometric diversity of low free energy Cu_4O_x clusters.

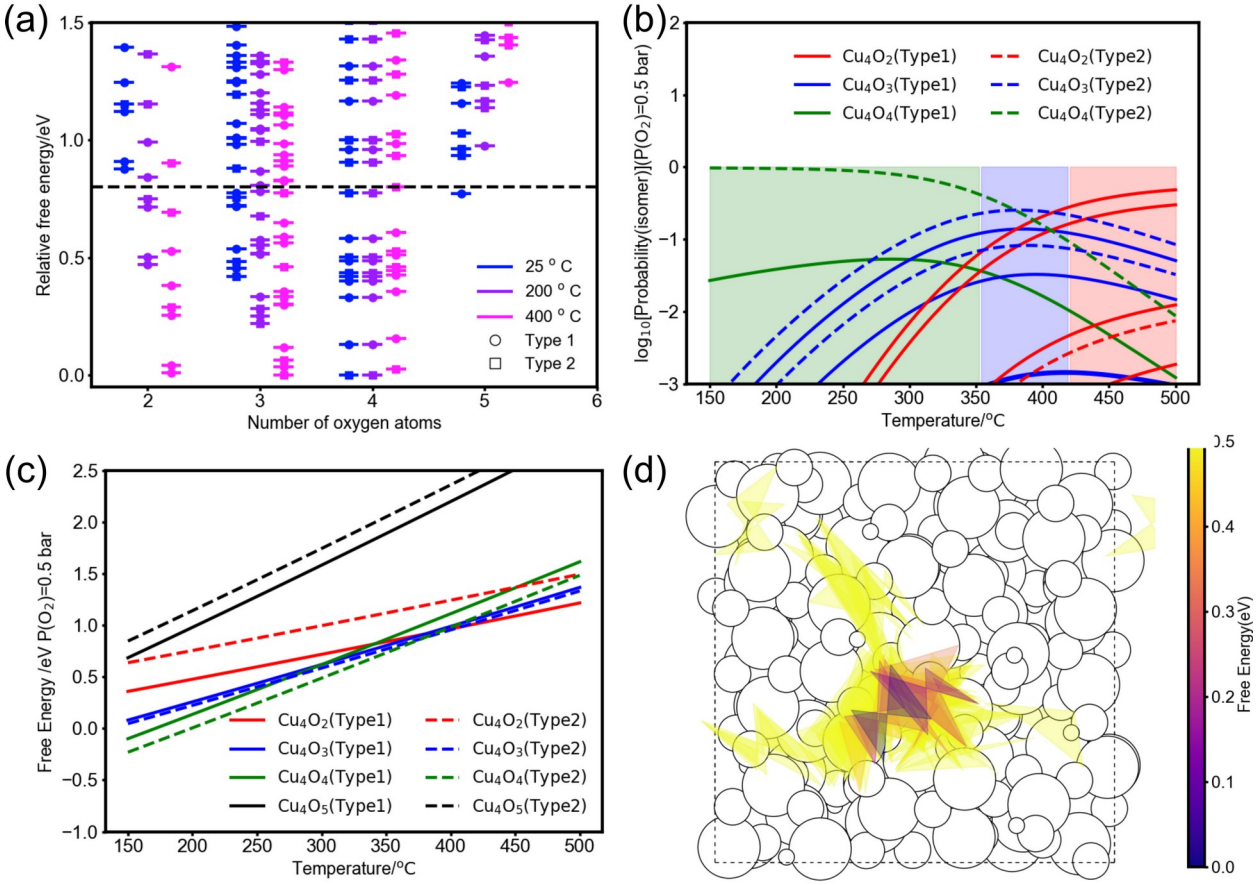

Figure 1 (a) Relative free energies (ΔG) of Cu_4O_x isomers on amorphous alumina as a function of the numbers of the oxygen atoms at three temperatures 25, 200 and 400 ℃. At each temperature, the ΔG are calculated using the relevant GM structure as a reference. The horizontal dash line is placed at 0.8 eV. (b) Occurrence probabilities of different isomers as a function of temperature estimated by the Boltzmann distribution normalized by the total occurrence; Background green (resp blue, red) colors indicate temperature regions where Cu_4O_4 (resp Cu_4O_3, Cu_4O_2) compositions dominate the ensemble; (c) Free energy of the most stable isomer for each stoichiometry and each cluster type as a function of temperature; (d) Location on the support for each isomer in the low free energy ensemble, shown by the projected positions of the four Cu atoms.

Because of the high potential diversity of geometries and stoichiometries of the clusters, the grand canonical basin hopping (GCBH) method is used to explore the configuration space and globally optimize the geometries and stoichiometry of Cu_4O_x clusters. The number of oxygen atoms are optimized in equilibrium with an O_2 reservoir at 200 ℃ and 0.5 bar O_2. Basin hoping moves consist of either a change of the coordinates of the cluster, or in a

variation of the O content by addition or removal of an O atom (or an O_2 molecule). This GCBH sampling results in a large diversity of structural isomers and stoichiometries, with 24 configurations in an interval of [0-0.8] eV from the GM, defined here as the low free energy ensemble (LFEE) (Figure 1(a) and Figure 2). Although diverse surface binding sites are available for grafting Cu_4O_x cluster on the amorphous alumina model support, low free energy configurations are bound in the vicinity of a specific surfaces site (Figure 1(d)). This suggests that cluster mobility is difficult on the oxide support, in link with the experimental evidence that clusters do not sinter in the considered oxidative conditions.[34, 52-53]

The GCBH approach generated a wide range of stoichiometries from Cu_4O_2 to Cu_4O_5, Cu_4O_2 to Cu_4O_4 being present in the LFEE in catalysis conditions (150-500 °C and 0.5 bar of O_2) with reasonable populations (Figure 1(b)). Cu_4O_5 is unstable under the considered conditions while Cu_4O_2 is only accessible at the high temperature end of our interval. Geometries of the Cu_4O_x clusters are open, with Cu atoms interacting with each other, or with the Al cations through oxygen and hydroxyl bridges (Figure 2). Cu-Cu coordination ranges on average from 1.5 to 2, compared to CuO bulk oxide (having Cu-Cu coordination of 12) and to a supposedly compact tetrahedron Cu_4 core bridged by oxygen atoms (Cu-Cu coordination 3). Two main types of structures can be distinguished (Figure S2 and Figure S3): type 1 have all Cu atoms above the supporting surface, and type 2 have one Cu atom intruding into the plane of the alumina surface, bearing high Cu-O coordination numbers (4 or 5 oxygen neighbors, Figure S4(d)), and featuring long Cu-O distances (mostly ¿2.0 *Å*, Figure S4(b)) as well as long Cu-Cu distances (mostly ¿3.5 *Å*, Figure S5(b)) with the other three Cu atoms. All the low free-energy isomers in Figure 2 contain hydroxyls, on the cluster or at its interface with the oxide, which come from the partially hydroxylated surface during the global optimization.

Considering that the diverse isomers are close in free energies, not only the most stable structure but also metastable ones could be populated at finite temperatures. Indeed, Figure 1(b) shows that several isomers, depending on the temperatures, can show a reasonable probability of presence. This is the case especially at temperatures in the range of 350 450℃ where at least two Cu_4O_3 isomers, one Cu_4O_4 and two Cu_4O_2 isomers show an occurrence probability larger than 10%. Hence, the catalyst is more appropriately represented by a mixture of several different Cu_4O_x isomers than by a stepwise reduction of single optimal isomer from Cu_4O_4 to Cu_4O_2, considering that isomerization is generally faster than the ODH reactions under considered conditions.[54-56]

The presence of several competitive Cu_4O_3 isomers not only results in a multiple-configuration catalyst at high temperature, but also alters the preferable stoichiometry of Cu_4O_x clusters as a function of temperature. Figure 1(b) shows that the phase transition temperature between Cu_4O_3 and Cu_4O_4 is T_{opt}=380℃, if only the optimal isomer of each stoichiometry is considered. However, the transition temperature that accounts for the sum of all isomers between Cu_4O_3 and Cu_4O_4 occurs earlier at $T_{ensemble}$=354℃. Similarly, the transition between Cu_4O_3 and Cu_4O_2 stability is shifted from 408 °C to 421 ℃ from the presence of several competitive Cu_4O_3 isomers. Though the precise agreement between such a prediction and experimental measurement is still challenging due to the approximate nature of the density functional, the impacts of clusters’

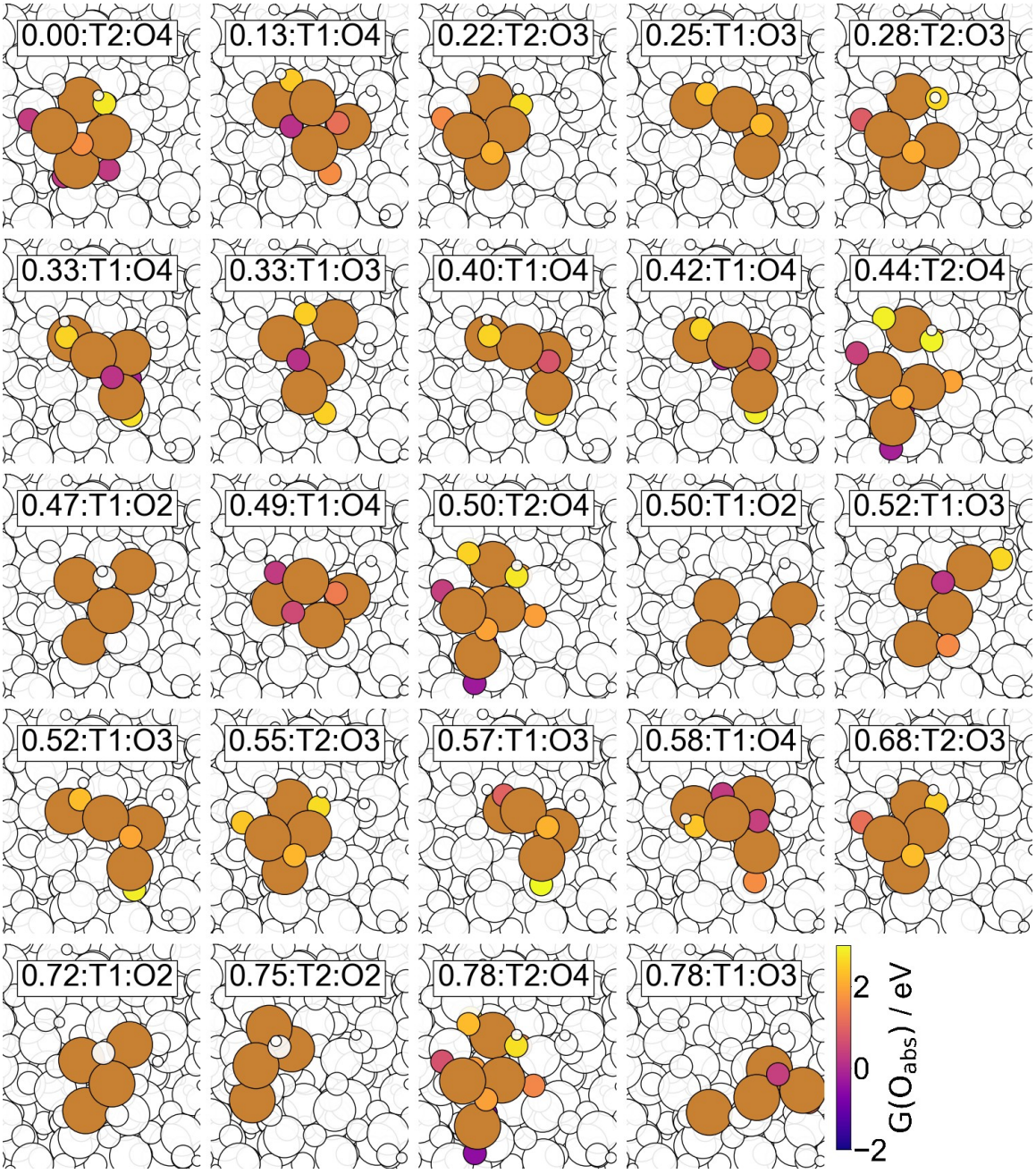

Figure 2 The structures of low free energy Cu_4O_x isomers of type 1 (noted as T1) or type 2 (noted as T2). The relative free energies of different isomers (G) as well as their stoichiometries (x, number of oxygen in the formula Cu_4O_x) are also indicated in the inserts (by the label of G:Tn:Ox). The brown balls are Cu atoms, The oxygen atoms, who contact with at least one Cu atom, are colored by the oxygen abstraction energy $\Delta G_{|¿^O|¿}$ if $\Delta G_{|¿^O|<3.0eV¿}$ (see text).

structural fluxionality on the description of the phase diagram is however an intrinsic property that must be taken into account for investigating the stabilities of similar system.[57]

If we consider type 1 and type 2 clusters separately, and assume that isomer equilibrium is seen only within the same type of isomers, the optimal stoichiometries of clusters of each type change with a similar trend, but the two types of Cu_4O_x clusters show different phase transition temperatures (Figure 1(c)). The transition from Cu_4O_4 to Cu_4O_3 takes place at 375 ℃ for type2, but at lower temperature of 301 ℃ for type1. On the other hand, type1 Cu_4O_3 get further reduced to Cu_4O_2 at around 376 ℃, but type2 Cu_4O_3 remains stable up to 500 ℃. Therefore, in cases where one Cu atom is inserted in the alumina plane, the cluster is generally more difficult to reduce. In this discussion on phase transformation, we assume, as so-far usually done, a complete thermodynamic equilibrium between the various configurations and composition, so that for example the Boltzmann weighted distribution of most stable Cu_4O_3 configurations transforms into that of Cu_4O_2 without any kinetic hindering.

3 Reducibilities of the Cu_4O_x clusters and their potential catalytic performance in selective oxidation reactions

To investigate the potential catalytic performances of the Cu_4O_x clusters in oxidation reactions, in which an oxygen atom will be abstracted from the Cu_4O_x cluster resulting in a reduced Cu_4O_{x-1} species, we calculated the free energy cost ($\Delta G_{\text{¿¿}}$ to remove an oxygen atom from the cluster, at 200 ℃ and 0.5 bar O_2. The reduced Cu_4O_{x-1} species is here only optimized to the nearest local minimum after O removal, as a way to model the structure of the catalyst after the oxidation reactions, which is not the optimal configuration of Cu_4O_{x-1}. Hence we do not consider only the low energy structures, as in the previous section, but also the intermediate structure for the reduced Cu_4O_{x-1} cluster along the reaction pathway, which might be high in energy and thus difficult to access. The O abstraction free energy is indicated by the color range on all structures (Figure 2) and the smallest

value (among different oxygen atoms of the same cluster) is shown as a function of cluster stability in Figure 3.

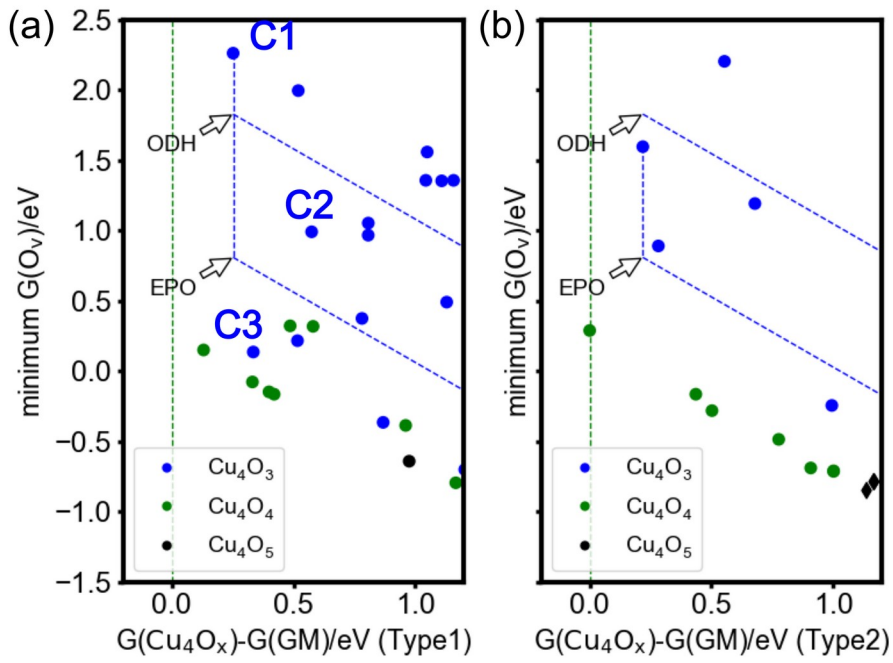

Figure 3: The smallest oxygen abstraction energy from each cluster versus the stability of the cluster. The left panel shows the results from clusters of type 1, and the right panel shows the results from clusters of type 2. The stabilities are illustrated by the relative free energies of each cluster using the GM as the reference. The two blue slanted dash lines in each panel show the boundary that separates clusters that would perform the specified oxidation reaction (propane oxidative dehydrogenation (ODH) or propene epoxidation (EPO)) exergonically (below the line) or endergonically (above) (See text and Supporting Information Table S2). The vertical green dash lines show the free energy of the GM.

The Cu_4O_x clusters on alumina present an extreme diversity in O abstraction energy values ranging from -1.2 to 5.1 eV depending on the isomer structure and stoichiometry. They first can strongly vary within a cluster and only those within $\Delta G_{|\Delta|<3.0eV}$ are shown in Figure 2. The minimal value on each cluster can also be very different among the isomers, as shown in Figure 3. Hence, the various isomers clearly present very different catalytic activities in oxidation. Generally, the Cu_4O_4 clusters show at least one O atom that is easy to abstract and they provide exergonic steps for propene epoxidation and propane ODH, used here as test reactions (Table S2). The first question is what is the formula of Cu_4O_x in the catalytic cycles: $Cu_4O_3 \leftrightarrow Cu_4O_5$ or $Cu_4O_2 \leftrightarrow Cu_4O_4$. This is indicated by the relative free energies of Cu_4O_x. All the

Cu_4O_5 clusters, which can be written as $Cu_4O_3(O_2)$ since all of them bear an O_2 dimer, are not stable with respect to O_2 desorption in the considered conditions (SI Section S3 and Figure S 6). Thus, the formation of Cu_4O_5 from Cu_4O_3 is difficult. This implies that the loop $Cu_4O_4 \rightarrow Cu_4O_3 \rightarrow Cu_4O_2 \rightarrow Cu_4O_4$ is the most promising catalytic cycle combining reduction of the Cu_4O_x cluster from the reaction and its further re-oxidation with O_2.

The reduction of Cu_4O_4 clusters is generally easy with a rather small $G_{|ċ^o|ċ}$. The removal of oxygen from the low free-energy Cu_4O_4 isomers also result in the formation of stable Cu_4O_3 isomers (shown in Figure S7). Especially for type 1 isomers, the reduction of the first four most stable Cu_4O_4 isomers produces the optimal Cu_4O_3 structure (C1 in Figure 3).

In contrast, the reducibility of Cu_4O_3 clusters is extremely isomer-specific. The lowest energy type 1 isomer (C1 in Figure 3(a)) shows large O abstraction energies (> 2.3 eV), and is unable to perform a step of propane ODH or propene epoxidation in an exergonic way. This most stable Cu_4O_3 isomer is a poor catalyst for oxidation, because upon O removal it produces a high-energy isomer of Cu_4O_2. However, low energy metastable isomers for Cu_4O_3, only 0.1-0.3 eV less stable than the GM, can provide much more reactive O atoms, with abstraction energy lowered to 1.0 eV (C2 in Figure 3) or even 0.14 eV (C3 in Figure 3). A potential rearrangement of the Cu_4O_3 cluster will produce a feasible oxidation reaction pathway for propane ODH or propene epoxidation. Considering an oxidation reaction from reactant R to product RO and accordingly reducing type1 Cu_4O_3 to Cu_4O_2, the reaction could take place first by the isomerization of the most stable $Cu_4O_3(C1)$ structure to a metastable isomer $Cu_4O_3(C2)$ (Figure 3(a)) which is more reducible and reacts with R forming the reduced structure Cu_4O_2 and the product RO. The overall reaction thermodynamics can be decomposed in the steps as shown below.

Reaction 1 $Cu_4O_3(C1) \rightarrow Cu_4O_3(C2)$ ΔG_{iso}

Reaction 2 $Cu_4O_3(C2) \rightarrow Cu_4O_2 + O$ $\Delta G_{¿?¿}$

Reaction 3 $R + O \rightarrow RO$ ΔG_{oxd}

The condition that the overall reaction is exergonic writes:

$$\Delta G_{iso} + \Delta G_{¿?¿} + \Delta G_{oxd} < 0.0¿ \quad (1)$$

In which, ΔG_{oxd} is fixed by the type of oxidation reaction, such as ODH of propane (ODH, -1.83 eV) or propene epoxidation (EPO, -0.81 eV) (see Supporting Information Table S2). Only those metastable isomers that satisfy Equation (1) will induce an exergonic reaction and they are located below the blue dashed boundary on Figure 3.

Hence, the selected promising type 1 candidates, which are able to provide an exothermic reaction step and also have a reasonable stability, are structure C2 and C3 in Figure 3(a). C2 can provide an exergonic oxidation reaction step for ODH and C3 can even provide an exergonic step for EPO. We investigated the pathways connecting C1 to C2 and C1 to C3 (Figure 4). Rearrangement proceeds with barriers of 0.58 eV and 1.36 eV, respectively, which can be overcome at a reasonable rate constant considering the high temperature of the reaction. The isomerization to C3 is slower, with a rate constant of 15 s^{-1}, using a standard prefactor, which is similar to the typical rate constant for the oxidation reaction step.[58] Therefore, the rearrangement between different Cu_4O_3 isomers provide an essential step for completing the catalytic cycles. This analysis is limited to type 1 isomers of Cu_4O_3, but a similar effect can be seen for Cu_4O_3 type 2 (Figure 3(b), blue points), where a weakly active most stable isomer bears a high O abstraction energy but a low energy metastable configuration is more active. However, the low energy type 2 Cu_4O_3 isomers are globally less reactive that the type 1 isomers, such as C3, for example.

We should note that in this analysis, O-removal barriers and associated kinetic effects are not considered. Reaction barriers depend on the specific reactant to be oxidized. Our reaction thermodynamics analysis clarifies the driving forces for exergonic reactions, which determines whether a reaction

could take place or not and setups the baseline to analyze the reaction mechanism.

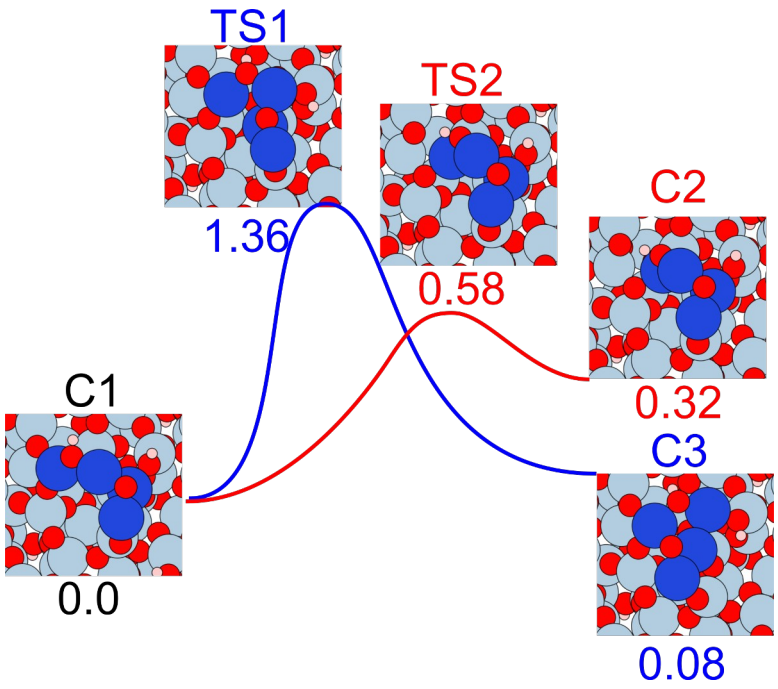

Figure 4 Pathways and transition state structures for the isomerization of Cu_4O_x from the stable but poorly reactive C1 to the reactive C2 and C3 configurations (Figure 3a).

4 Novel Cu environments in small Cu_4O_x clusters.

The analysis of the geometric and electronic structures of the supported Cu_4O_x clusters provides insight into their unique character compared with their bulk counterparts. The Cu-O bond lengths for the clusters are in the range 1.8 2.2 $\AA$ (Figure S4), which is close to the first-neighbor Cu-O bond lengths in the bulk Cu_2O (1.85 Å) and CuO (1.96 Å). However, the first-neighbor Cu-Cu bond lengths are quite diverse in the Cu_4O_x clusters (Figure S5), especially in the Cu_4O_3 clusters of type 1. The shortest Cu-Cu bond lengths in Cu_4O_3 of type 1 are around 2.25 Å, which is much smaller than that in the bulk CuO (3.08 Å) and Cu_2O (3.02 Å), or even in the Cu metal (2.55 Å) (Figure S5). In addition, the short Cu-Cu separations are accompanied by an 'abnormal' intermediate Bader charges on Cu in the range of 0.6 0.8$|e|$, which is very different from that of the Cu atoms in Cu_2O (0.54 $|e|$) and CuO

(0.99 $|e|$) (Figure S8-10). Those specific Bader charges and bond lengths imply very unique electronic properties of supported Cu_4O_x clusters.

Oxygen atoms present a diverse anionic nature in the cluster isomers. In the Cu_3O_4 clusters, nucleophilic O atoms with marked ionic character are characterized by very large abstraction energies, and thus, a poor catalytic activity for oxidation, while electrophilic O atoms with small charge are highly active (Figure 5). These electrophilic O atoms showing small oxygen abstraction energies are also bonded with Cu neighbors with intermediate charge, i.e. in a mixed-valence state. Such electrophilic O atoms are not seen in the bulk or at the surface of Cu oxides, explaining the specific reactivity of nano-size clusters.

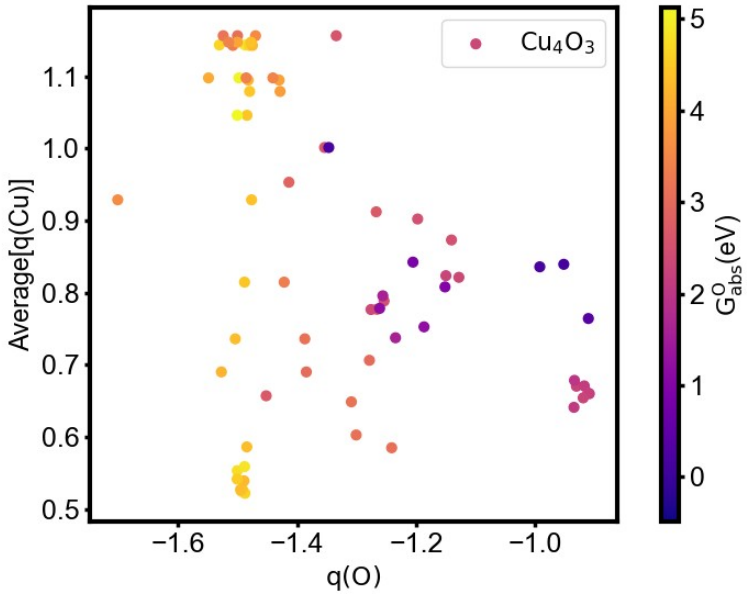

Figure 5: Abstraction energies for O atoms on Cu_4O_3 isomers, shown as the color scale, as a function of charge on the O atom and average charge on the neighboring Cu centers.

5 Conclusion

Small partially oxides Cu clusters, the size 4 being studied here, present a variety of oxidation levels depending on the oxygen partial pressure and

temperature, a result which is fully expected. In the reaction conditions ($P(O_2)$ = 0.5 bar, T=200-400 °C) Cu_4O_4 and Cu_4O_3 are the most stable compositions. However, each composition is not associated with one well-defined structure but with an ensemble of low energy isomers, accessible at the high temperature of the reaction. More surprisingly, these low energy isomers can present significantly different catalytic activities in catalyzed reactions of oxidation. This is especially the case for the Cu_4O_3 composition, where the most stable isomers are inactive for oxidation, as judged by the oxygen abstraction energies, while low energy metastable isomers can contain O atoms with an abstraction energy reduced by more than 2 eV, and are much more active for oxidation. Pathways with sizeable but reasonable barriers, considering the reaction temperature, connect the inactive low energy and the active metastable isomers. Oxygen atoms of less ionic nature, bound the mixed-valence Cu atoms, generally present the smallest abstraction energies.

Cu_4O_4 clusters are reactive for oxidation, even in their most stable isomer. The loop $Cu_4O_4 \rightarrow Cu_4O_3 \rightarrow Cu_4O_2 \rightarrow Cu_4O_4$ appears as the most efficient catalytically, as judged from its thermodynamics. All low energy isomers of Cu_4O_4 of type 1 connect after reduction to the most stable C1 isomer of Cu_4O_3. However, this isomer is inactive for oxidation, because upon losing O it would produce a high-energy isomer of Cu_4O_2. Therefore, isomerization to a metastable configuration of Cu_4O_3, such as C2 or C3, is a key part of the mechanism, enabling to perform the second oxidation step. The Cu_4O_2 cluster is then re-oxidized by O_2 is an exothermic step at the considered temperature.

Reorganization of the structure of the Cu_4O_x cluster during catalytic oxidation cycle is concluded to be crucial for the reaction, and a static cluster would not be active. Compared to the case of metallic clusters (such as Pt clusters), the barriers for isomerization are significantly higher, since the O atoms in the cluster make them more rigid.[14] These barriers remain smaller than, or

comparable to the typical ODH barrier on oxides (~1.6 eV).[58] Thus, it cannot be excluded, that in some cases, this reorganization event could be involved as the rate-limiting step in the reaction.

6 Methods:

6.1 Grand Canonical Basin Hopping

The GCBH explorations are carried out by an in-house code, which is developed based on Atomic Simulation Environment (ASE) package.[59] GCBH explores the configuration and composition space simultaneously to minimize following targeted function, which is the free energy (or formation energy) of the supported Cu_4O_x cluster at specific condition of O_2

$$G\left(Cu_4O_x@a-Al_2O_3\right)=E\left(Cu_4O_x@a-Al_2O_3\right)-\sum_{j=1}^{M_{species}}\mu_j N_j \qquad (2)$$

In Equation (2) , $E\left(Cu_4O_x@a-Al_2O_3\right)$ is the DFT calculated electronic energy of the system which is approximated as the free energy of the slab. Therefore, the vibrational contributions are ignored for slab systems considering that those contributions are small.[60] μ_j is the chemical potential of element type j and N_j is the number of element type j in the system. In this work, only N_{Oxygen} is variable. The oxygen is assumed in equilibrium with the O_2 gas at 200 ℃ and a partial pressure of 0.5 bar.

15 amorphous alumina supported Cu_4O_x are used as initial inputs. x is randomly chosen from 2 to 5 and the locations of the clusters are also randomly selected. 15 GCBHs explorations are launched in parallel to minimize the free energies supported clusters by a series of basin hopping steps. Each GCBH step consists of three steps: (a) generating new structure from the previous local minimum, (b) local optimization, and (c) the rule to accept or reject new structure. The method to generate new structures uses one of the four approaches: 1) randomly displacing the Cartesian positions of the atoms within the Cu_4O_x cluster by a small distance; 2) adding an oxygen atom near the randomly selected Cu atom; 3) adding an O_2 molecule

near the randomly selected Cu site; 4) randomly removing an oxygen atom from the Cu_4O_x cluster. Note that we did not implement the systematic exploration of the support reconstruction, though the top layers of the support are allowed to relax along with the configuration changes of the Cu_4O_x clusters (Figure S11). With this choice, the surface mounted cluster configurations are extensively sampled, while structures where Cu_4O_x may intrude into the support receive a smaller focus. The new generated structure is then optimized in step (b) by BFGS algorithm implemented in ASE until the maximum force exerted on atoms is below 0.03 eV/Angstrom. Finally, in step (c) the probability to accept the new structure is determined by Metropolis algorithm, i.e. the acceptance probability is $p=min\left[1.0,\exp\left(\frac{-G_{i+1}-G_i}{k_BT}\right)\right]$, in which G_{i+1} and G_i are the free energies of new and old optimized structures. The temperature $T=1500\,K$ is used as a parameter throughout this work. Note that the high T(=1500 K) here is only used for calculating BH acceptance probability ensuring that the sampling will not converge too quickly, hence being different from the temperature of the O_2 reservoir. A prototype example for the efficiency of implemented GCBH is demonstrated in Figure S12.

6.2 DFT Calculation Details

DFT calculations are carried out using VASP package.[61-64] For VASP calculations, the projector augmented wave (PAW) pseudopotentials are used for describing the core electrons. Valence orbitals are expanded with plane wave basis sets up to 400 eV.[65] Spin polarized calculations are always used to take into account the spin multiplicities. Perdew–Burke–Ernzerhof (PBE) functional is exploited to calculate the electronic exchange correlation energies.[66] It is known that the *d* orbitals of Cu present so-called strong self-interaction, hence the on-site coulomb interaction is introduced by Hubbard model[67] with U=7.0 eV for the *d* orbitals of Cu (see benchmark in the

Supporting information). The PBE-induced binding energy error for O_2 is also accounted for, by treating the chemical potential of oxygen as a parameter that is fitted against the hybrid functional, HSE06 (See supporting information). The amorphous alumina model is from a previous paper of Cheng et al[68], which exploits force-field based molecular dynamics simulations.[69-70] The slab is orthogonal with dimension of $15.56 \times 15.56 Å^2$, and it has a formula of $H_{16}Al_{68}O_{110}$. Transition states are firstly located by NEB[71] method and then refined by DIMER[72] method until the maximum force residue is smaller than 0.03 eV/Å. TSs are finally confirmed to present only one imaginary frequency.

7 Supporting information

This information is available free of charge on the ACS Publications website. Computational details, Experimental thermodynamics values, Classification of Cu_4O_x clusters by grafting site, Analysis of the Cu's coordination with O atoms for Cu_4O_x clusters, Analysis of the Cu-Cu distance distribution, Bader charges and geometries, Oxygen abstracting energies of low free energy ensemble of Cu_4O_x clusters, sideview of slab model, prototype example for GCBH, atomic coordinates for the 24 LFEE structures.

8 Acknowledgments

This work was funded by DOE-BES grant DE-SC0019152. This work used computational and storage services associated with the Hoffman2 Shared Cluster provided by UCLA Institute for Digital Research and Education's Research Technology Group. This research used resources of the National Energy Research Scientific Computing Center (NERSC), a U.S. Department of Energy Office of Science User Facility operated under Contract No. DE-AC02-05CH11231. An award of computer time was provided by the Innovative and Novel Computational Impact on Theory and Experiment (INCITE) program. This research used resources of the Argonne Leadership Computing Facility,

which is a DOE Office of Science User Facility supported under Contract DE-AC02-06CH11357.

9 References

1. Tyo, E. C.; Vajda, S., Catalysis by clusters with precise numbers of atoms. *Nat. Nanotech.* **2015,** *10*, 577.
2. Vajda, S.; Pellin, M. J.; Greeley, J. P.; Marshall, C. L.; Curtiss, L. A.; Ballentine, G. A.; Elam, J. W.; Catillon-Mucherie, S.; Redfern, P. C.; Mehmood, F.; Zapol, P., Subnanometre platinum clusters as highly active and selective catalysts for the oxidative dehydrogenation of propane. *Nature Materials* **2009,** *8*, 213.
3. Lei, Y.; Mehmood, F.; Lee, S.; Greeley, J.; Lee, B.; Seifert, S.; Winans, R. E.; Elam, J. W.; Meyer, R. J.; Redfern, P. C.; Teschner, D.; Schlögl, R.; Pellin, M. J.; Curtiss, L. A.; Vajda, S., Increased Silver Activity for Direct Propylene Epoxidation via Subnanometer Size Effects. *Science* **2010,** *328* (5975), 224-228.
4. Maeno, Z.; Kibata, T.; Mitsudome, T.; Mizugaki, T.; Jitsukawa, K.; Kaneda, K., Subnanoscale Size Effect of Dendrimer-encapsulated Pd Clusters on Catalytic Hydrogenation of Olefin. *Chem. Lett.* **2011,** *40* (2), 180-181.
5. Zandkarimi, B.; Alexandrova, A. N., Dynamics of Subnanometer Pt Clusters Can Break the Scaling Relationships in Catalysis. *J. Phys. Chem. Lett.* **2019,** *10* (3), 460-467.
6. Musselwhite, N.; Alayoglu, S.; Melaet, G.; Pushkarev, V. V.; Lindeman, A. E.; An, K.; Somorjai, G. A., Isomerization of n-Hexane Catalyzed by Supported Monodisperse PtRh Bimetallic Nanoparticles. *Catal. Lett.* **2013,** *143* (9), 907-911.
7. Sun, X.; Lin, J.; Chen, Y.; Wang, Y.; Li, L.; Miao, S.; Pan, X.; Wang, X., Unravelling platinum nanoclusters as active sites to lower the catalyst loading for formaldehyde oxidation. *Commun. Chem.* **2019,** *2* (1).
8. Lee, J. H.; Cho, J.; Jeon, M.; Ridwan, M.; Park, H. S.; Choi, S. H.; Nam, S. W.; Han, J.; Lim, T.-H.; Ham, H. C.; Yoon, C. W., Experimental and computational studies of formic acid dehydrogenation over PdAu: influence of ensemble and ligand effects on catalysis. *J. Mater. Chem. A* **2016,** *4* (37), 14141-14147.
9. Liu, L.; Corma, A., Metal Catalysts for Heterogeneous Catalysis: From Single Atoms to Nanoclusters and Nanoparticles. *Chem. Rev.* **2018,** *118* (10), 4981-5079.
10. Schmid, G.; Baumle, M.; Geerkens, M.; Helm, I.; Osemann, C.; Sawitowski, T., Current and future applications of nanoclusters. *Chem. Soc. Rev.* **1999,** *28* (3), 179-185.
11. Hakkinen, H.; Abbet, S.; Sanchez, A.; Heiz, U.; Landman, U., Structural, electronic, and impurity-doping effects in nanoscale chemistry: supported gold nanoclusters. *Angew. Chem. Int. Ed. Engl.* **2003,** *42* (11), 1297-300.
12. Zhai, H.; Alexandrova, A. N., Ensemble-Average Representation of Pt Clusters in Conditions of Catalysis Accessed through GPU Accelerated Deep Neural Network Fitting Global Optimization. *J. Chem. Theory Comput.* **2016,** *12* (12), 6213-6226.
13. Zhai, H.; Alexandrova, A. N., Fluxionality of Catalytic Clusters: When It Matters and How to Address It. *ACS Catal.* **2017,** *7* (3), 1905-1911.
14. Zhai, H.; Alexandrova, A. N., Local Fluxionality of Surface-Deposited Cluster Catalysts: The Case of Pt7 on Al2O3. *J. Phys. Chem. Lett.* **2018,** *9* (7), 1696-1702.
15. Sun, G.; Sautet, P., Metastable Structures in Cluster Catalysis from First-Principles: Structural Ensemble in Reaction Conditions and Metastability Triggered Reactivity. *J. Am. Chem. Soc.* **2018,** *140* (8), 2812-2820.
16. Gao, M.; Lyalin, A.; Takagi, M.; Maeda, S.; Taketsugu, T., Reactivity of Gold Clusters in the Regime of Structural Fluxionality. *J. Phys. Chem. C* **2015,** *119* (20), 11120-11130.
17. Halder, A.; Ha, M.-A.; Zhai, H.; Yang, B.; Pellin, M. J.; Seifert, S.; Alexandrova, A. N.; Vajda, S., Oxidative Dehydrogenation of Cyclohexane by Cu vs Pd Clusters: Selectivity Control by Specific Cluster Dynamics. *ChemCatChem* **2019,** *12*, 1-10.
18. Ha, M.-A.; Baxter, E. T.; Cass, A. C.; Anderson, S. L.; Alexandrova, A. N., Boron Switch for Selectivity of Catalytic Dehydrogenation on Size-Selected Pt Clusters on Al2O3. *J. Am. Chem. Soc.* **2017,** *139* (33), 11568-11575.
19. Baxter, E. T.; Ha, M.-A.; Cass, A. C.; Alexandrova, A. N.; Anderson, S. L., Ethylene Dehydrogenation on $Pt_{4,7,8}$ Clusters on Al_2O_3: Strong Cluster Size Dependence Linked to Preferred Catalyst Morphologies. *ACS Catal.* **2017,** *7* (5), 3322-3335.

20. Fukuda, R.; Sakai, S.; Takagi, N.; Matsui, M.; Ehara, M.; Hosokawa, S.; Tanaka, T.; Sakaki, S., Mechanism of NO–CO reaction over highly dispersed cuprous oxide on γ-alumina catalyst using a metal–support interfacial site in the presence of oxygen: similarities to and differences from biological systems. *Catal. Sci. Technol.* **2018,** *8* (15), 3833-3845.
21. Yin, G.; Nishikawa, M.; Nosaka, Y.; Srinivasan, N.; Atarashi, D.; Sakai, E.; Miyauchi, M., Photocatalytic Carbon Dioxide Reduction by Copper Oxide Nanocluster-Grafted Niobate Nanosheets. *ACS Nano* **2015,** *9* (2), 2111-2119.
22. Grundner, S.; Markovits, M. A.; Li, G.; Tromp, M.; Pidko, E. A.; Hensen, E. J.; Jentys, A.; Sanchez-Sanchez, M.; Lercher, J. A., Single-site trinuclear copper oxygen clusters in mordenite for selective conversion of methane to methanol. *Nat. Chem.* **2015,** *6*, 7546.
23. Li, G.; Vassilev, P.; Sanchez-Sanchez, M.; Lercher, J. A.; Hensen, E. J. M.; Pidko, E. A., Stability and reactivity of copper oxo-clusters in ZSM-5 zeolite for selective methane oxidation to methanol. *J. Catal.* **2016,** *338*, 305-312.
24. Woertink, J. S.; Smeets, P. J.; Groothaert, M. H.; Vance, M. A.; Sels, B. F.; Schoonheydt, R. A.; Solomon, E. I., A $[Cu_2O]^{2+}$ core in Cu-ZSM-5, the active site in the oxidation of methane to methanol. *Proc. Natl. Acad. Sci. USA* **2009,** *106* (45), 18908-13.
25. Brezicki, G.; Kammert, J. D.; Gunnoe, T. B.; Paolucci, C.; Davis, R. J., Insights into the Speciation of Cu in the Cu-H-Mordenite Catalyst for the Oxidation of Methane to Methanol. *ACS Catal.* **2019**, 5308-5319.
26. Jayamurthy, M.; Hayden, P.; Bhattacharya, A. K., Direct catalytic epoxidation of ethene over copper and alumina-supported copper. *J. Catal.* **2014,** *309*, 309-313.
27. Yang, X. F.; Kattel, S.; Xiong, K.; Mudiyanselage, K.; Rykov, S.; Senanayake, S. D.; Rodriguez, J. A.; Liu, P.; Stacchiola, D. J.; Chen, J. G., Direct Epoxidation of Propylene over Stabilized Cu^+ Surface Sites on Titanium-Modified Cu_2O. *Angew. Chem. Int. Ed.* **2015,** *54* (41), 11946-11951.
28. Marimuthu, A.; Zhang, J.; Linic, S., Tuning Selectivity in Propylene Epoxidation by Plasmon Mediated Photo-Switching of Cu Oxidation State. *Science* **2013,** *339* (6127), 1590-1593.
29. Torres, D.; Lopez, N.; Illas, F.; Lambert, R. M., Why Copper Is Intrinsically More Selective than Silver in Alkene Epoxidation: Ethylene Oxidation on Cu(111) versus Ag(111). *J. Am. Chem. Soc.* **2005,** *127* (31), 10774-10775.
30. Su, W.; Wang, S.; Ying, P.; Feng, Z.; Li, C., A molecular insight into propylene epoxidation on Cu/SiO_2 catalysts using O_2 as oxidant. *J. Catal.* **2009,** *268* (1), 165-174.
31. Hua, Q.; Cao, T.; Gu, X. K.; Lu, J. Q.; Jiang, Z. Q.; Pan, X. R.; Luo, L. F.; Li, W. X.; Huang, W. X., Crystal-Plane-Controlled Selectivity of Cu_2O Catalysts in Propylene Oxidation with Molecular Oxygen. *Angew. Chem. Int. Ed.* **2014,** *53* (19), 4856-4861.
32. Nauert, S. L.; Rosen, A. S.; Kim, H.; Snurr, R. Q.; Stair, P. C.; Notestein, J. M., Evidence for Copper Dimers in Low-Loaded CuO_x/SiO_2 Catalysts for Cyclohexane Oxidative Dehydrogenation. *ACS Catal.* **2018,** *8* (10), 9775-9789.
33. Tyo, E. C.; Yin, C.; Di Vece, M.; Qian, Q.; Kwon, G.; Lee, S.; Lee, B.; DeBartolo, J. E.; Seifert, S.; Winans, R. E.; Si, R.; Ricks, B.; Goergen, S.; Rutter, M.; Zugic, B.; Flytzani-Stephanopoulos, M.; Wang, Z. W.; Palmer, R. E.; Neurock, M.; Vajda, S., Oxidative Dehydrogenation of Cyclohexane on Cobalt Oxide (Co_3O_4) Nanoparticles: The Effect of Particle Size on Activity and Selectivity. *ACS Catal.* **2012,** *2* (11), 2409-2423.
34. Mammen, N.; Spanu, L.; Tyo, E. C.; Yang, B.; Halder, A.; Seifert, S.; Pellin, M. J.; Vajda, S.; Narasimhan, S., Using first principles calculations to interpret XANES experiments: extracting the size-dependence of the (p , T) phase diagram of sub-nanometer Cu clusters in an O_2 environment. *J. Phys. Condens. Matter.* **2019,** *31* (14), 144002.
35. Yang, B.; Yu, X.; Halder, A.; Zhang, X.; Zhou, X.; Mannie, G. J. A.; Tyo, E.; Pellin, M. J.; Seifert, S.; Su, D.; Vajda, S., Dynamic Interplay between Copper Tetramers and Iron Oxide Boosting CO_2 Conversion to Methanol and Hydrocarbons under Mild Conditions. *ACS Sustain. Chem. Eng.* **2019,** *7* (17), 14435-14442.
36. Grajciar, L.; Heard, C. J.; Bondarenko, A. A.; Polynski, M. V.; Meeprasert, J.; Pidko, E. A.; Nachtigall, P., Towards operando computational modeling in heterogeneous catalysis. *Chem. Soc. Rev.* **2018,** *47* (22), 8307-8348.
37. Calvo, F.; Schebarchov, D.; Wales, D. J., Grand and Semigrand Canonical Basin-Hopping. *J Chem Theory Comput* **2016,** *12* (2), 902-9.
38. Wales, D. J.; Doye, J. P. K., Global Optimization by Basin-Hopping and the Lowest Energy Structures of Lennard-Jones Clusters Containing up to 110 Atoms. *J. Phys. Chem. A* **1997,** *101* (28), 5111-5116.
39. Revard, B. C.; Tipton, W. W.; Yesypenko, A.; Hennig, R. G., Grand-canonical evolutionary algorithm for the prediction of two-dimensional materials. *Phy. Rev. B* **2016,** *93* (5).

40. Tipton, W. W.; Hennig, R. G., A grand canonical genetic algorithm for the prediction of multi-component phase diagrams and testing of empirical potentials. *J. Phys. Condens. Matter.* **2013,** *25* (49), 495401.
41. Mendes, P. S. F.; Chizallet, C.; Pérez-Pellitero, J.; Raybaud, P.; Silva, J. M.; Ribeiro, M. F.; Daudin, A.; Bouchy, C., Interplay of the adsorption of light and heavy paraffins in hydroisomerization over H-beta zeolite. *Catal. Sci. Technol.* **2019,** *9* (19), 5368-5382.
42. Kurisingal, J. F.; Rachuri, Y.; Palakkal, A. S.; Pillai, R. S.; Gu, Y.; Choe, Y.; Park, D.-W., Water-Tolerant DUT-Series Metal–Organic Frameworks: A Theoretical–Experimental Study for the Chemical Fixation of CO2 and Catalytic Transfer Hydrogenation of Ethyl Levulinate to γ-Valerolactone. *ACS Appl. Mater. Interfaces* **2019,** *11* (44), 41458-41471.
43. Kirchhoff, B.; Braunwarth, L.; Jung, C.; Jónsson, H.; Fantauzzi, D.; Jacob, T., Cuboctahedral Platinum Nanoparticles: Simulations of the Oxidation and Degradation of Platinum Electrocatalysts (Small 5/2020). *Small* **2020,** *16* (5), 2070027.
44. Senftle, T. P.; van Duin, A. C. T.; Janik, M. J., Methane Activation at the Pd/CeO2 Interface. *ACS Catal.* **2017,** *7* (1), 327-332.
45. Sun, G.; Alexandrova, A. N.; Sautet, P., Pt8 cluster on alumina under a pressure of hydrogen: Support-dependent reconstruction from first-principles global optimization. *J. Chem. Phys.* **2019,** *151* (19), 194703.
46. Liu, J.-X.; Su, Y.; Filot, I. A. W.; Hensen, E. J. M., A Linear Scaling Relation for CO Oxidation on CeO_2-Supported Pd. *J. Am. Chem. Soc.* **2018,** *140* (13), 4580-4587.
47. Heyd, J.; Scuseria, G. E.; Ernzerhof, M., Hybrid functionals based on a screened Coulomb potential. *J. Chem. Phys.* **2003,** *118* (18), 8207-8215.
48. Krukau, A. V.; Vydrov, O. A.; Izmaylov, A. F.; Scuseria, G. E., Influence of the exchange screening parameter on the performance of screened hybrid functionals. *J. Chem. Phys.* **2006,** *125* (22), 224106.
49. Heinemann, M.; Eifert, B.; Heiliger, C., Band structure and phase stability of the copper oxides Cu_2O, CuO, and Cu_4O_3. *Phys. Rev. B* **2013,** *87* (11), 115111.
50. Xu, X. L.; Yang, B.; Wei, Z. Y.; Cao, G. J.; Xu, H. G.; Zheng, W. J., Structural and bonding properties of Cu3O3- and Cu3O4- clusters: anion photoelectron spectroscopy and density functional calculations. *Physical Chemistry Chemical Physics* **2018,** *20* (31), 20622-20628.
51. Bae, G.-T.; Dellinger, B.; Hall, R. W., Density Functional Calculation of the Structure and Electronic Properties of Cu_nO_n (n = 1−8) Clusters. *J. Phys. Chem. A* **2011,** *115* (11), 2087-2095.
52. Yang, B.; Liu, C.; Halder, A.; Tyo, E. C.; Martinson, A. B. F.; Seifert, S.; Zapol, P.; Curtiss, L. A.; Vajda, S., Copper Cluster Size Effect in Methanol Synthesis from CO2. *J. Phys. Chem. C* **2017,** *121* (19), 10406-10412.
53. Mammen, N.; Spanu, L.; Tyo, E. C.; Yang, B.; Halder, A.; Seifert, S.; Pellin, M. J.; Vajda, S.; Narasimhan, S., Reversing Size-Dependent Trends in the Oxidation of Copper Clusters through Support Effects. *Eur. J. Inorg. Chem.* **2018,** *2018* (1), 16-22.
54. Nauert, S. L.; Schax, F.; Limberg, C.; Notestein, J. M., Cyclohexane oxidative dehydrogenation over copper oxide catalysts. *J. Catal.* **2016,** *341*, 180-190.
55. Dinse, A.; Khennache, S.; Frank, B.; Hess, C.; Herbert, R.; Wrabetz, S.; Schlögl, R.; Schomäcker, R., Oxidative dehydrogenation of propane on silica (SBA-15) supported vanadia catalysts: A kinetic investigation. *J. Mol. Catal. Chem.* **2009,** *307* (1), 43-50.
56. Chen, K.; Bell, A. T.; Iglesia, E., Kinetics and Mechanism of Oxidative Dehydrogenation of Propane on Vanadium, Molybdenum, and Tungsten Oxides. *J. Phys. Chem. B* **2000,** *104* (6), 1292-1299.
57. Zhang, Z.; Jimenez-Izal, E.; Hermans, I.; Alexandrova, A. N., Dynamic Phase Diagram of Catalytic Surface of Hexagonal Boron Nitride under Conditions of Oxidative Dehydrogenation of Propane. *J. Phys. Chem. Lett.* **2019,** *10* (1), 20-25.
58. Sattler, J. J. H. B.; Ruiz-Martinez, J.; Santillan-Jimenez, E.; Weckhuysen, B. M., Catalytic Dehydrogenation of Light Alkanes on Metals and Metal Oxides. *Chem. Rev.* **2014,** *114* (20), 10613-10653.
59. Hjorth Larsen, A.; Jorgen Mortensen, J.; Blomqvist, J.; Castelli, I. E.; Christensen, R.; Dulak, M.; Friis, J.; Groves, M. N.; Hammer, B.; Hargus, C.; Hermes, E. D.; Jennings, P. C.; Bjerre Jensen, P.; Kermode, J.; Kitchin, J. R.; Leonhard Kolsbjerg, E.; Kubal, J.; Kaasbjerg, K.; Lysgaard, S.; Bergmann Maronsson, J.; Maxson, T.; Olsen, T.; Pastewka, L.; Peterson, A.; Rostgaard, C.; Schiotz, J.; Schutt, O.; Strange, M.; Thygesen, K. S.; Vegge, T.; Vilhelmsen, L.; Walter, M.; Zeng, Z.; Jacobsen, K. W., The atomic simulation environment-a Python library for working with atoms. *J. Phys. Condens. Matter.* **2017,** *29* (27), 273002.
60. Reuter, K.; Scheffler, M., Composition, structure, and stability of RuO_2(110) as a function of oxygen pressure. *Phys. Rev. B* **2001,** *65* (3), 035406.

61. Kresse, G.; Furthmüller, J., Efficiency of ab-initio total energy calculations for metals and semiconductors using a plane-wave basis set. *Comput. Mater. Sci.* **1996,** *6* (1), 15-50.
62. Kresse, G.; Furthmüller, J., Efficient iterative schemes forab initiototal-energy calculations using a plane-wave basis set. *Phys. Rev. B* **1996,** *54* (16), 11169-11186.
63. Kresse, G.; Hafner, J., Ab initiomolecular dynamics for liquid metals. *Phys. Rev. B* **1993,** *47* (1), 558-561.
64. Kresse, G.; Hafner, J., Ab initiomolecular-dynamics simulation of the liquid-metal–amorphous-semiconductor transition in germanium. *Phys. Rev. B* **1994,** *49* (20), 14251-14269.
65. Kresse, G.; Joubert, D., From ultrasoft pseudopotentials to the projector augmented-wave method. *Phys. Rev. B* **1999,** *59* (3), 1758-1775.
66. Perdew, J. P.; Burke, K.; Ernzerhof, M., Generalized Gradient Approximation Made Simple. *Phys. Rev. Lett.* **1996,** *77* (18), 3865-3868.
67. Dudarev, S. L.; Botton, G. A.; Savrasov, S. Y.; Humphreys, C. J.; Sutton, A. P., Electron-energy-loss spectra and the structural stability of nickel oxide: An LSDA+U study. *Phy. Rev. B* **1998,** *57* (3), 1505-1509.
68. Cheng, L.; Yin, C.; Mehmood, F.; Liu, B.; Greeley, J.; Lee, S.; Lee, B.; Seifert, S.; Winans, R. E.; Teschner, D.; Schlögl, R.; Vajda, S.; Curtiss, L. A., Reaction Mechanism for Direct Propylene Epoxidation by Alumina-Supported Silver Aggregates: The Role of the Particle/Support Interface. *ACS Catal.* **2013,** *4* (1), 32-39.
69. Adiga, S. P.; Zapol, P.; Curtiss, L. A., Atomistic simulations of amorphous alumina surfaces. *Physical Review B* **2006,** *74* (6).
70. Adiga, S. P.; Zapol, P.; Curtiss, L. A., Structure and Morphology of Hydroxylated Amorphous Alumina Surfaces. *J. Phys. Chem. C* **2007,** *111* (20), 7422-7429.
71. Henkelman, G.; Jónsson, H., Improved tangent estimate in the nudged elastic band method for finding minimum energy paths and saddle points. *J. Chem. Phys.* **2000,** *113* (22), 9978-9985.
72. Henkelman, G.; Jónsson, H., A dimer method for finding saddle points on high dimensional potential surfaces using only first derivatives. *J. Chem. Phys.* **1999,** *111* (15), 7010-7022.